Journal of the Optical Society of America A
OPTICS, IMAGE SCIENCE, AND VISION

Overlap relation between free-space Laguerre Gaussian modes and step-index fiber modes

Robert Brüning,[1] Yingwen Zhang,[2] Melanie McLaren,[3] Michael Duparré,[1] and Andrew Forbes[3,*]

[1]Institute of Applied Optics, Abbe Center of Photonics, Friedrich Schiller University Jena, Fröbelstieg 1, D-07743 Jena, Germany
[2]Council for Scientific and Industrial Research, National Laser Center, P.O. Box 395, Pretoria 0001, South Africa
[3]School of Physics, University of the Witwatersrand, Private Bag 3, Johannesburg 2050, South Africa
*Corresponding author: andrew.forbes@wits.ac.za

Received 19 June 2015; revised 29 July 2015; accepted 29 July 2015; posted 30 July 2015 (Doc. ID 243373); published 20 August 2015

We investigated the overlap relation of the free-space Laguerre–Gaussian modes to the corresponding linearly polarized modes of a step-index fiber. To maximize the overlap for an efficient coupling of the free-space modes into a fiber, the scale-dependent overlap was theoretically and experimentally determined. The presented studies pave the way for further improvement of free-space to fiber optical connections. © 2015 Optical Society of America

OCIS codes: (060.2310) Fiber optics; (090.1760) Computer holography; (140.3295) Laser beam characterization.

http://dx.doi.org/10.1364/JOSAA.32.001678

1. INTRODUCTION

Multi-mode fibers (MMF) are widely used in a plethora of applications, such as optical sensors [1], fiber lasers [2], and optical communication [3]. Besides the possibility of all-fiber devices, the connection between the fiber and its supported modes with the free-space modes is important to control the optical properties of the emerging beam or the excited field distributions at the fiber input. The simplest connection is given by fibers with a parabolic refractive index profile, typical of graded-index fibers, whose modes can be described by Laguerre–Gaussian (LG) functions and are solutions of the free-space wave equation [4]. However, in all other cases, the fiber modes do not match the free-space solutions, resulting in no stable propagation of the emerging beams in free space. In addition, in general, free-space modes are not suitable to excite selective pure fiber modes, and additional beam shaping techniques are required, such as the use of computer generated holograms [5]. The main disadvantages of such beam shaping techniques are low efficiency and the fact that they result in high transformation losses. For the common type of step-index fibers, which show the same cylindrical symmetry as in free-space, it is possible to approximate the fiber modes by suitable free-space modes [6].

In this paper, we investigate the approximation of step-index fiber modes by free-space modes theoretically as well as experimentally, to evaluate the quality and the limitation of this approach. We determine the overlap relation between both mode sets as a function of the scale parameter for the free space, as well as the fiber parameter, V. For the theoretical investigations, we develop an analytical solution for this overlap problem, which allows us to study a wide parameter range. Additionally, we investigate experimentally the overlap relation by applying the correlation filter method [7] and verify the analytical solution. Our results will be of interest to studies in which fiber to free-space links are necessary.

2. FUNDAMENTALS

At the transition from free space to fiber, and vice versa, one always has mode coupling between the free-space modes on the one side and the fiber modes on the other. To achieve a maximized coupling efficiency and a low crosstalk between modes of different orders, the scaling of the free-space beam has to be adapted to the fiber.

In the case of a weakly guiding step-index fiber, the fiber modes are given by the linearly polarized (LP) mode set. For that, the field distribution, $F_{\ell p}(r,\varphi)$, is given by the solution of the scalar Helmholtz equation. Considering a cylindrically symmetric fiber with a core radius a, the solution is given by [4]

$$\mathrm{LP}_{\ell p}(r,\varphi) = N_{\ell p}\begin{cases} J_\ell\left(\frac{\nu_{\ell p} r}{a}\right)/J_\ell(\nu_{\ell p}) & \text{for } r < a \\ K_\ell\left(\frac{\mu_{\ell p} r}{a}\right)/K_\ell(\mu_{\ell p}) & \text{for } r \geq a \end{cases} \times e^{i\ell\varphi}, \tag{1}$$

where $N_{\ell p}$ is a normalization constant, J_ℓ denotes the ℓth-order Bessel function of the first kind, and K_ℓ denotes the ℓth-order modified Bessel function of the second kind, with $\nu_{\ell p}$ and $\mu_{\ell p}$ being the normalized propagation constants of

the core and cladding, respectively. The exact expression for the normalization constant is derived in Appendix A. For the description of the LP modes, the additional fiber parameter V is required, which is defined as

$$V^2 = \nu^2 + \mu^2 = \left(\frac{2\pi}{\lambda}a\right)^2 (n_{\text{core}}^2 - n_{\text{cladding}}^2), \tag{2}$$

where n_{core} and n_{cladding} are the refractive indices of the core and cladding material, respectively. This fiber parameter defines the amount of modes and their propagation constants.

Since the step-index fiber has cylindrical symmetry, the adapted free-space mode set is given by the LG modes, which are the solutions of the paraxial Helmholtz equation in a cylindrically symmetric coordinate system. For that, the solution at the waist position is given by

$$\text{LG}_{p\ell}(r,\varphi) = M_{p\ell}\left(\frac{2r^2}{w_0^2}\right)^{\frac{|\ell|}{2}} L_p^{|\ell|}\left(\frac{2r^2}{w_0^2}\right) e^{-\frac{r^2}{w_0^2}} e^{i\ell\varphi}, \tag{3}$$

where $L_p^{|\ell|}$ are the associated Laguerre polynomials, w_0 is the fundamental Gaussian radius, and $M_{p\ell} = \frac{1}{w_0}\left(\frac{2p!}{\pi(\ell+p)!}\right)^{\frac{1}{2}}$ is a normalization factor.

Comparing the modes described by Eq. (1) and Eq. (3), we notice that they show the same azimuthal dependence and a characterization of the radial order by the amount of root points in the intensity distribution. Hence, corresponding modes can be found by choosing the same azimuthal order and the field functions with the same amount of roots in radial direction.

Since both mode sets differ in the actual shape of the radial function, an adaption of the scale parameters is needed for the best possible matching of both mode sets. The matching of the scale can be evaluated by the overlap relation:

$$\eta_n = \iint \text{LG}_n(r,\varphi)\text{LP}_n^*(r,\varphi)\mathrm{d}A, \tag{4}$$

where η_n defines the amount of power that is coupled from one mode into the other at the transition between both mode sets. It can reach values between one when the fields are perfectly matched, and zero for orthogonal fields. The amount of power $1-\eta_n$ which is not coupled into the desired mode goes in other nonorthogonal, reflecting, or radiating modes to satisfy energy conservation.

3. ANALYTICAL ANALYSIS

To optimize the mode overlap, we derive an analytical expression for the overlap relation as a function of the mode parameters. First, we separate the problem into a core and a cladding part, corresponding to the solution of the fiber modes Eq. (1). The $e^{i\ell\varphi}$ term ensures that the LP and LG modes must have the same azimuthal index ℓ. Hence, to solve the overlap relation, the radial part of Eq. (4) becomes the important one.

For deriving the solution for the core region, we note that the Bessel function of the first kind can be written as an infinite sum,

$$J_\ell(x) = \sum_{m=0}^{\infty} \frac{(-1)^m}{m!\Gamma(m+\ell+1)}\left(\frac{x}{2}\right)^{2m+\ell}, \tag{5}$$

with Γ the gamma function, whereas the Laguerre polynomial can be written as its generating function,

$$L_p^{|\ell|}(x) = \frac{1}{p!}\left(\frac{d}{d\xi}\right)^p \frac{1}{(1-\xi)^{|\ell|+1}} \exp\left(\frac{-x\xi}{1-\xi}\right)\bigg|_{\xi=0}. \tag{6}$$

Using Eq. (5) and Eq. (6) for the description of the mode function, Eq. (1) and Eq. (3), respectively, the overlap of both mode sets within the core is given by

$$\begin{aligned}\eta_{\ell p}^{\text{core}} = {} & \frac{N_{\ell p}}{J_\ell(\nu)}\frac{M_{p\ell}}{p!}(\sqrt{2})^\ell \left(\frac{d}{d\xi}\right)^p \frac{1}{(1-\xi)^{|\ell|+1}} \\ & \times \sum_{m=0}^{\infty}\left\{\frac{(-1)^m}{m!\Gamma(m+\ell+1)}\left(\frac{\nu w_0}{2a}\right)^{2m+\ell}\left(\frac{1-\xi}{1+\xi}\right)^{m+\ell+1}\right. \\ & \left.\times\left[\Gamma(m+\ell+1) - \Gamma\left(m+\ell+1, \frac{a^2}{w_0^2}\frac{1+\xi}{1-\xi}\right)\right]\right\}\bigg|_{\xi=0},\end{aligned} \tag{7}$$

with $\Gamma(a,z)$ being the incomplete gamma function; $N_{\ell p}$ and $M_{p\ell}$ being the normalization constant of the LP and LG modes, respectively; a being the fiber core radius; and w_0 being the Gaussian radius.

For the cladding region, an analytical solution for the overlap integral can be found by a similar approach. For that, we make use of the following relation between modified Bessel functions of the second kind K_ℓ and the modified Bessel functions of the first kind I_ℓ:

$$K_\ell(x) = \lim_{n\to\ell}\frac{\pi}{2\sin(n\pi)}[I_{-n}(x) - I_n(x)], \tag{8}$$

where the I_n can be written as an infinite sum,

$$I_n(x) = \sum_{m=0}^{\infty}\frac{1}{m!\Gamma(m+n+1)}\left(\frac{x}{2}\right)^{2m+n}. \tag{9}$$

Using Eq. (8) and Eq. (9) to describe the field distribution of the fiber modes in the cladding region, together with the previously used representation of the LG modes given by Eq. (3) and Eq. (6), the overlap of the cladding part becomes

$$\begin{aligned}\eta_{\ell p}^{cl} = {} & \lim_{n\to\ell}\frac{\pi}{2\sin(n\pi)}\frac{N_{\ell p}}{K_n(\mu)}\frac{M_{p\ell}}{p!}(\sqrt{2})^n\left(\frac{d}{d\xi}\right)^p \\ & \times\frac{1}{(1-\xi)^{|\ell|+1}}\sum_{m=0}^{\infty}\left\{\frac{-1}{m!}\left(\frac{\mu w_0}{2a}\right)^{2m-\ell}\left(\frac{1-\xi}{1+\xi}\right)^{m+1}\right. \\ & \times\left[\frac{\Gamma\left(m+n+1, \frac{a^2}{w_0^2}\frac{1+\xi}{1-\xi}\right)}{\Gamma(m+n+1)}\left(\frac{\mu w_0}{2a}\right)^{2n}\left(\frac{1-\xi}{1+\xi}\right)^n\right. \\ & \left.\left.\times\frac{\Gamma\left(m+1, \frac{a^2}{w_0^2}\frac{1+\xi}{1-\xi}\right)}{\Gamma(m-n+1)}\right]\right\}\bigg|_{\xi=0}.\end{aligned} \tag{10}$$

The complete overlap relation of core and cladding is then given by the sum of Eqs. (7) and (10).

4. CORRELATION FILTER ANALYSIS

For a direct measurement of the overlap relation between the LP and the corresponding LG modes, the correlation filter method (CFM) was used. This optically performs the integral relation given by Eq. (4) and allows the experimental investigation of the overlap between LP and LG modes [7].

The experimental setup used for measuring the scale-dependent overlap relation is shown in Fig. 1. A plane wave has illuminated a phase-only spatial light modulator (SLM). Applying the phase-only coding technique for complex valued field distributions proposed by Arrizòn *et al.* [8] enables the shaping of arbitrarily scaled LG modes. The generated LG modes were then imaged by a telescopic 4f setup onto the correlation filter (CF), which had the field distribution of the LP modes implemented as the transmission function. The CF was realized by a static binary computer generated hologram, where the encoding technique by Lee [9] was used, since, for the CF, no dynamic change of the transmission function was required. After an optical Fourier transformation with a lens in 2f configuration, the correlation signal was accessible at the CCD sensor as the intensity value on the optical axis, which was proportional to the overlap relation between both modes.

Since the encoding method of the hologram required all the generated LG modes to be normalized to unit amplitude, energy conservation is, therefore, violated. To ensure the comparability of the measured results by an appropriated power scaling, a correction parameter for each encoded field was introduced, which followed by the renormalization of the mode fields. The encoded mode fields, $\tilde{\psi}_n(\mathbf{r})$, differ from the basis mode fields, $\psi_n(\mathbf{r})$, by a constant factor, $\tilde{\psi}_n(\mathbf{r}) = \psi_n(\mathbf{r})/\alpha_n$, where $\alpha_n = \max\{|\psi_n(\mathbf{r})|\}$. An appropriate power scaling and correction of the measured intensities I_{meas} were achieved by multiplying it by the square of the correction parameter α_n to produce the normalized intensity $I_{\text{norm}} = I_{\text{meas}}\alpha_n^2$ [5]. Finally, the measured and corrected overlap values have to be normalized to one, which is given by the overlap between the LP mode with itself. For that, the LP mode encoded in the CF was generated with the SLM, and the measured intensity was used to normalize the overlap relations obtained for the different scaled LG modes.

This procedure for the generation of dynamically scaled LG modes and the evaluation of the overlap with a set of LP modes with a fixed scale enable the measurement of the scale-dependent relation between both mode sets.

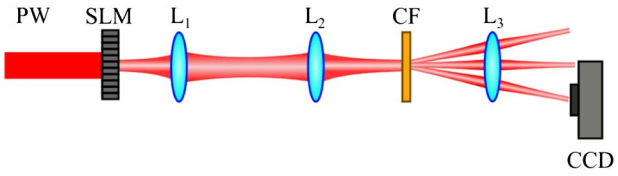

Fig. 1. Experimental setup for the measurement of the overlap relation between the LP and LG modes, where the LG modes are generated with the SLM and decomposed by the CFM. PW, plane wave; SLM, spatial light modulator; L_{1-3}, lenses; CCD, camera.

5. RESULTS

We applied the correlation filter method onto an LP mode set with an underlying V parameter of 4.72, resulting in the appearance of six guided modes. In Fig. 2, the experimentally measured scale-dependent overlap is shown, together with the theoretical curve calculated by our analytical solution. It can be seen that, for all LP modes of the investigated fiber, the corresponding LG modes are good approximations at a beam-to-core radius ratio of 0.75. In this fiber, the overlap is about 0.99 for the LP_{01}, LP_{11} and, LP_{21} modes, and about 0.98 for the LP_{02} mode. A comparison of the scale-dependent overlap of the four fiber modes shows explicit differences between them. Noticeable are the differences in the rate of decrease of the overlap when the LG mode sizes are not ideal, whereas for the fundamental mode, LP_{01}, the overlap falls relatively slowly, while the higher-order modes show an obvious faster decline. Additionally, the optimal ratio between beam width and core radius for maximal overlap differs slightly for the investigated modes from 0.70 for the LP_{21} [see Fig. 2(d)], up to 0.81 for the fundamental mode LP_{01} [see Fig. 2(a)]. Further, the maximal reachable overlap for the higher-order radial, LP_{02}, mode [see Fig. 2(b)] with about 0.98 slightly lower compared to the other modes. Since the comparison between the experimental and theoretical results showed a good agreement that demonstrates the reliability of our method, we used the theoretical expressions to study further the influences of the mode order or the V parameter on the overlap relation.

As seen in Fig. 2, the overlap relation changes in shape, maximum position, and maximum value for different modes.

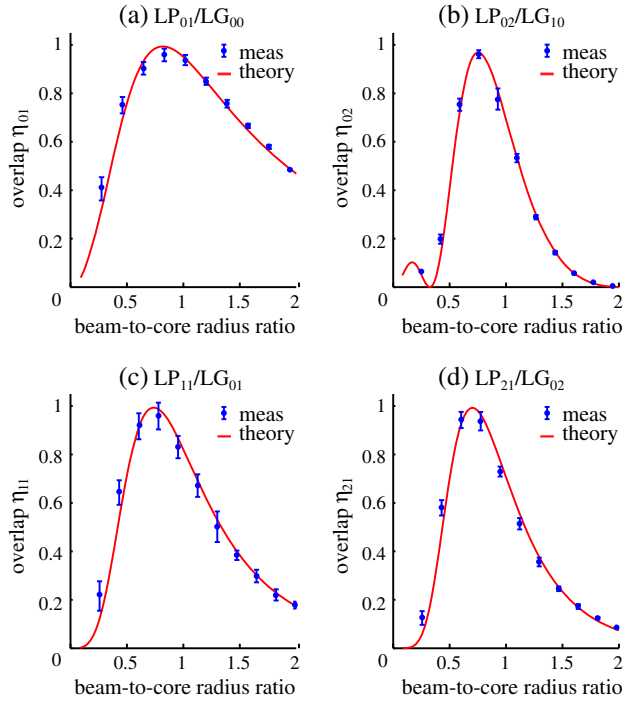

Fig. 2. Comparison between theoretical and experimental determined overlap relation.

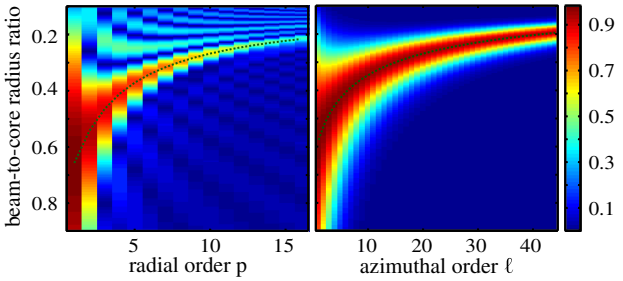

Fig. 3. Size-dependent overlap relation for modes with increasing radial and azimuthal order. The trend of the optimal beams size is highlighted by the green line.

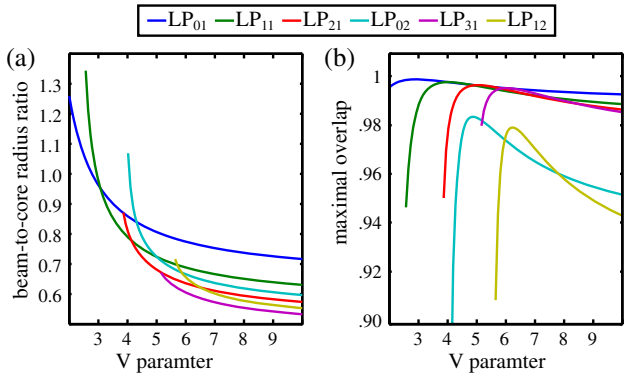

Fig. 4. V parameter dependence of the overlap relation between the LP and corresponding LG modes. (a) Optimal ratio between the Gaussian beam width and the core radius for a maximized overlap. (b) Maximal achievable overlap in dependence of V.

This means that there is always an optimal match, based on the fundamental Gaussian beam size, for the corresponding LG mode set. Applying our analytical expression, we have determined the scale-dependent overlap for different higher-order modes for a fiber with $V = 50$ to demonstrate some effects. As shown in Fig. 3 for higher-order radial modes with azimuthal index $\ell = 0$ and higher-order azimuthal mode with radial index $p = 1$, the position of the optimal beam size becomes smaller with increasing azimuthal and radial indices. This behavior is as expected since the beam width of LG modes of higher order follows $w = w_0\sqrt{2p + \ell + 1}$ with w_0 the Gaussian width, while, on the other hand, the LP modes are well confined within the core resulting in a decrease of the needed Gaussian width to match the scale of the corresponding modes. A second effect which can be seen is that the region with high overlap shrinks with increasing mode order, and a good adaptation of the scale parameters becomes more crucial. Especially for modes of higher radial order, the maximal achievable overlap decreases with increasing mode order, indicating the limits of the applied approximation. Hence, the approximation of the LP modes of the step-index fiber by LG modes cannot be extended for arbitrary higher-order modes. Therefore, an acceptable coupling loss has to be considered in possible applications where higher-order modes are used. Nevertheless, the results demonstrate that the low-order LP modes can be accurately approximated by LG modes.

Additionally, we investigated the influence of the underlying V-parameter on the quality of our suggested approximation. We have calculated the optimal beam-to-core radius ratio and the maximal achievable overlap for different modes as a function of the V parameter, as shown in Fig. 4. In Fig. 4(a), the change of the optimal beam-to-core radius ratio is depicted. It can be seen that, for low V values, in the case of LP_{01} or V values close to the cutoff of a mode, the optimal beam-to-core ratio becomes larger than one indicating the bad confinement of the mode inside the core. For increasing V values, optimal beam-to-core ratio rapidly decreases. In Fig. 4(b), it can be seen that, when V increases and moves away from the cutoff of a mode, the maximum overlap of that mode rapidly increases to a peak, then slowly starts to decrease. This drop in the maximum overlap is faster for higher-order modes.

Finally, we have also compared the intensity profiles of LG and LP modes with maximum overlap. Four possible modes for a fiber with a V parameter of 4.72 can be seen in Fig. 5, where the different mode profiles are normalized to unit intensity for easier comparison. It can be seen clearly that the conformity decreases with increasing mode order. Figure 5(a) illustrates that the profiles of the fundamental modes, LP_{01} and LG_{00}, are well matched, whereas the distinctions become more significant for the higher-order modes. For modes of higher-azimuthal order, such as the LP_{11} and LG_{01} modes shown in Fig. 5(b), the maxima of the ring-like intensity pattern are slightly displaced. In addition for higher-order radial modes, structural differences occur, such as the displacement of the minima and the side lobe maxima, as seen in Fig. 5(c). The distinction becomes more prevalent with increasing mode order, as seen in Fig. 5(d) for the higher-order radial and azimuthal modes, LP_{12} and LG_{21}, where the side lobes show notable deviations resulting in a lower achievable overlap relation.

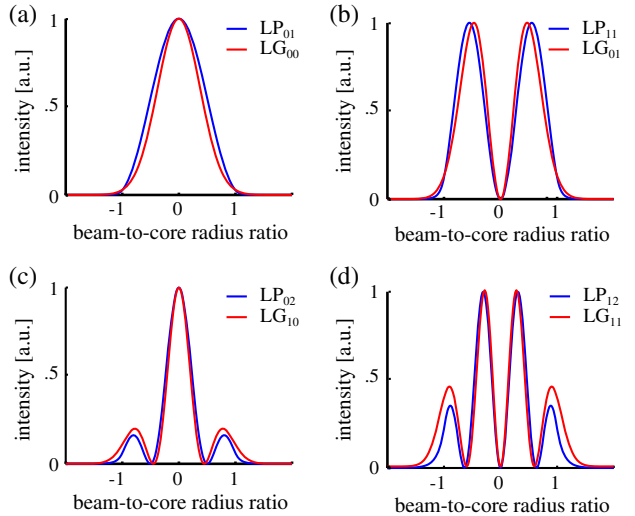

Fig. 5. Comparison of the intensity profiles between the LP modes and the corresponding LG modes for the maximized overlap.

6. CONCLUSION

We have shown that the LP modes of a step-index fiber can be approximated by a scale-adapted set of LG free-space modes. The validity of this approximation is shown experimentally for a fiber with a V parameter of 4.72. Further, we used an analytical solution of the overlap problem to investigate the limits of the approach for a wide spectrum of the LP modes and V parameters. We have found that the approximation is good but with certain limitations, which are set by the requirements on acceptable coupling losses and mode purity of the specific application. To provide high overlap, the LP modes have to be far from their cutoff condition and of low radial order. Additionally, the optimal beam-to-core radius ratio changes for each corresponding mode pair. For a low V fiber with few allowed modes (such as the example fiber), this dependence is weak, and a good approximation of all modes can be found for an appropriately adapted LG mode set. In the case of highly multimode fibers, the LG mode set has to be optimized individually for each corresponding mode pair or at least for different groups of them.

APPENDIX A

To evaluate the overlap relation between the LG and LP modes, we also need an analytical expression for the normalization constant, N_{lp}, in Eq. (1). For that, we use the normalization condition,

$$1 = \iint \mathrm{LP}_{\ell p}(r,\varphi)\mathrm{LP}^{*}_{\ell p}(r,\varphi)\mathrm{d}A, \tag{A1}$$

which gives

$$N^2_{\ell p} = \frac{1}{2\pi}\left\{\frac{\int_0^a \left[J_\ell\left(\frac{\nu_{\ell p} r}{a}\right)\right]^2 r\mathrm{d}r}{|J_\ell(\nu_{\ell p})|^2} + \frac{\int_a^\infty \left[K_\ell\left(\frac{\mu_{\ell p} r}{a}\right)\right]^2 r\mathrm{d}r}{|K_\ell(\mu_{\ell p})|^2}\right\}^{-1}. \tag{A2}$$

The integrals are evaluated to be

$$2\pi\int_0^a \left[J_\ell\left(\frac{\nu r}{a}\right)\right]^2 r\mathrm{d}r = \frac{\pi a^2}{\nu_{\ell p}}[\nu J_\ell(\nu)^2 - 2lJ_\ell(\nu)J_{\ell+1}(\nu) + \nu J_{\ell+1}(\nu)^2] \tag{A3}$$

and

$$\begin{aligned}2\pi\int_a^\infty \left[K_\ell\left(\frac{\mu r}{a}\right)\right]^2 r\mathrm{d}r = \lim_{n\to\ell}\frac{\pi^2 a^2}{4\mu^2\sin(n\pi)^2}\{&\pi\mu^2 I_{1-n}(\mu^2) \\ &+2\pi\mu I_{1-n}(\mu)[-\mu I_{n-1}(\mu) + nI_n(\mu)] \\ &-\pi\mu I_{-n}(\mu)^2 + \pi[2n\mu I_{n-1}(\mu)I_n(\mu) \\ &-(4n^2+\mu^2)I_n(\mu)^2 + \mu^2 I_{1+n}(\mu)^2] \\ &+2\mu I_{-n}(\mu)[2nK_{1-n}(\mu)\sin(n\pi) \\ &+\pi\mu I_n(\mu)]\},\end{aligned} \tag{A4}$$

with $I_n(x)$ being the modified Bessel function of the first kind. Inserting Eqs. (A3) and (A4) into Eq. (A2) yields the analytical expression for the normalization constant for the solution of the overlap relation for the core and cladding region, Eqs. (7) and (10), respectively.

Acknowledgment. The authors thank Darryl Naidoo for technical assistance and Sigmund Schröter for fabrication of the correlation filter.

REFERENCES

1. B. Lee, "Review of the present status of optical fiber sensors," Opt. Fiber Technol. **9**, 57–79 (2003).
2. S. Ramachandran, J. Fini, M. Mermelstein, J. Nicholson, S. Ghalmi, and M. Yan, "Ultra-large effective-area, higher-order mode fibers: a new strategy for high-power lasers," Laser Photon. Rev. **2**, 429–448 (2008).
3. G. Li, N. Bai, N. Zhao, and C. Xia, "Space-division multiplexing: the next frontier in optical communication," Adv. Opt. Photon. **6**, 413–487 (2014).
4. A. W. Snyder and J. D. Love, *Optical Waveguide Theory* (Chapman & Hall, 1996).
5. D. Flamm, C. Schulze, D. Naidoo, S. Schröter, A. Forbes, and M. Duparré, "All-digital holographic tool for mode excitation and analysis in optical fibers," J. Lightwave Technol. **31**, 1023–1032 (2013).
6. R. Brüning, S. Ngcobo, M. Duparré, and A. Forbes, "Direct fiber excitation with a digitally controlled solid state laser source," Opt. Lett. **40**, 435–438 (2015).
7. T. Kaiser, D. Flamm, S. Schröter, and M. Duparré, "Complete modal decomposition for optical fibers using CGH-based correlation filters," Opt. Express **17**, 9347–9356 (2009).
8. V. Arrizón, U. Ruiz, R. Carrada, and L. A. González, "Pixelated phase computer holograms for the accurate encoding of scalar complex fields," J. Opt. Soc. Am. A **24**, 3500–3507 (2007).
9. W. H. Lee, "Sampled Fourier transformed hologram generation by computer," Appl. Opt. **9**, 639–643 (1970).